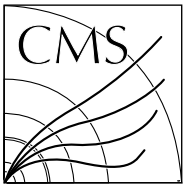

The Compact Muon Solenoid Experiment

CMS Note

Mailing address: CMS CERN, CH-1211 GENEVA 23, Switzerland

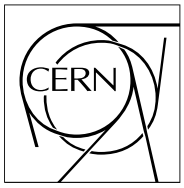

2 July 1997

The possibility of jet modelling at the CMS test beam experiments

V.V. Abramov

Institute for High Energy Physics, Protvino, Moscow Region 142284, Russia

Abstract

The problem of a jet modelling at the CMS test beam experiments has been studied using GEANT 3.21 package. A simple experimental set-up consisting of an active target and a hodoscope in the forward hemisphere is proposed to separate spectator jets from single particles which passed the target without interaction. The rejection factor of proposed algorithm for single particles is better then 1000 in the energy range from 10 to 1000 GeV. Efficiency of jet detection in the same energy range is about 70% or better. The proposed algorithm of jet selection allows one to study response of calorimeters and other detectors on jets and single particles using existing test beams.

1 Introduction

The major purpose of detectors in collider experiments is to detect products of hard particle collisions. Most of produced particles are grouped into jet like objects which are considered in theory as manifestation of quark and gluon fragmentation. Quarks which did not take part in hard collisions produce so called spectator jets. They are produced at small angles around colliding beams direction. All jets are collimated into cones which became narrower with the rise of jet energy.

Experimental study of detector performance at test beam facilities is usually done only for single particles. Selection of high P_T jets in fixed target experiments presents a very complicated problem since their cross section is very small and jets are emitted at very small angles in the laboratory frame, where they overlap with a spectator jet.

On the other hand spectator jets are produced with high probability in each inelastic event and they can be used to study various detectors, in particular the CMS calorimeters. A simple experimental set-up is proposed for selection of spectator jets in a test beam experiment. A sketch of the experimental set-up is shown in Fig. 1. It includes an active target consisting of Beryllium plates of 1 cm thickness and of 4 mm thick scintillator counters situated after the plates. Total number of Be plates is 8 and transverse size of the plates is 20*20 cm^2. A sketch of the target is shown in Fig. 2. A total thickness of the target and its material (0.25 Λ_{INT}, 0.30 X_0) are chosen so that secondary interactions in it do not change significantly momentum distribution and multiplicity of particles produced in the primary interaction.

Another important part of the set-up is a circular shape hodoscope (STRG) shown in detail in Fig. 3. It consist of 8 concentric 4 mm thick scintillator rings with minimum radius equal to 2 cm, and maximum radius equal to 40 cm. The distance of the hodoscope from the target is 80 cm. The hodoscope elements are not divided in azimuth angle to have fewer channels, though such division can increase its ability to select jets.

Information about energy depositions in the active target and in each channel of hodoscope STRG is used to reject events in which incident particle did not interact in the target or have elastic interaction. The detail description of the algorithm is presented in the following section.

2 Selection of spectator jets

Several variable were used to reject single particles and select spectator jets which are produced by incident hadrons in the active target. For the purpose of Monte Carlo study of jet selection algorithm all generated events are divided into three classes using GEANT [1] information which is generally not available in experiment. Pions with momenta 10, 25, 50, 100, 200, 500 and 1000 GeV/c were used as probe particles.

The first class (17.6% of all events) includes events in which incident particles strongly interacted in the target and produce a jet like bunch of particles in the forward direction called below jets. The criteria which is used to select such events is

$$\delta_{CH} = E_{CH}/E_{TOT} < 0.995, \tag{1}$$

where E_{CH} and E_{TOT} are kinetic energies of charged particles and all particles after the target, respectively. Distribution of all generated events vs δ_{CH} is shown in Fig. 4. The spike in Fig. 4 corresponds to events for which incident particle has no inelastic interaction in the target. Events below the spike corresponds to spectator jets. Charged particle multiplicity corresponding eq. (1) is shown in Fig. 5.

The second class (single particles, no interaction in the target) of events was selected by conditions:

$$\delta_{CH} = E_{CH}/E_{TOT} > 0.995; \quad N_{CH} = 1; \;\; N_{PH} = 0, \tag{2}$$

where N_{CH} and N_{PH} are multiplicities of charged particles and photons, respectively. The third class of events includes all events which are not included into the first two classes. Most of these events have low charged multiplicity and are close in properties to class 2 events.

Several variables are used in the experimental algorithm of jet selection and single particle rejection. One of them is energy deposition (E_{TAG}) in the target. Distribution of E_{TAG} for jets (class 1) and single particle (class 2) events are shown in Fig. 6 and Fig. 7, respectively. Cut $E_{TAG} > 0.03$ GeV suppress single particle events by a factor around 50.

Another variable is R_{STRG} which means an average radius of fired counters in the hodoscope STRG, where weight

for each counter is proportional to energy deposition in it:

$$R_{STRG} = \Sigma R_i \cdot E_i / \Sigma E_i. \quad (3)$$

Distributions of R_{STRG} for jets and single particle events are shown in Fig. 8 and Fig. 9, respectively. Selection cut $R_{STRG} > 3$ cm alone is already good enough to suppress single particle events by one order of magnitude. A small fraction of class 2 events have large R_{STRG} due to soft neutrons produced in pion-nucleus interactions.

The number of fired counters in the hodoscope (N_{STRG}) with energy deposition above some threshold is another useful variable. For threshold equal to zero N_{STRG} distributions for jets and single particles are shown Fig. 10 and Fig. 11, respectively. Selection cut $N_{STRG} > 0$ alone suppress single particle events by one order of magnitude.

Total energy deposition in the hodoscope (E_{STRG}) gives additional tool for suppression of single particle events. Its distribution for jets and single particle events are shown in Fig. 12 and Fig. 13, respectively. Selection cut $E_{STRG} > 0.007$ GeV alone suppress single particle events by two orders of magnitude.

The final algorithm for jet selection includes all the above variables and additional parameter CUT which is used to increase thresholds for different variables simultaneously. Selection is done by assigning a weight $W = 1$ for each event, if all of the conditions below is satisfied:

- a) $E_{STRG} > 0.007 * CUT$ (GeV);
- b) $R_{STRG} > 3 * CUT$ (cm);
- c) $N_{STRG} > min(1, CUT)$;
- d) $E_{TAG} > 0.03 * CUT$ (GeV).

If at least one of conditions (a,b,c,d) is not satisfied, event has weight $W = 0$ and is not accepted as a jet. Numerical parameters in conditions (a,b,c,d) are chosen to have optimal cuts for all variables with CUT value around unity.

The use of combination of cuts gives very powerful criteria for suppression of single particle events and at the same time selects jets with high probability. This is illustrated in Fig. 14 and Fig. 15 for jets and single particle events, respectively. The variable CUT shown in these figures is proportional to thresholds used for each of the above variables. If CUT is around 0.7, jets are selected with efficiency about 70%, and single particle events are suppressed by three orders of magnitude or better. Since the rejection power of the algorithm is very high, we can use the active target without Berillium plates at all and have still a clean jet sample. Jet class events rejected by the selection algorithm have low charged multiplicity (< 10).

Efficiency of the algorithm for class 3 events (17.9% of total events) is shown in Fig. 16 as a function of CUT. Class 3 events are suppressed by two orders of magnitude if $CUT > 1$. Charged multiplicity for class 3 events before application of the jet selection algorithm is shown in Fig. 17. The mean multiplicity is 1.7 which is very low compared with 14.8 value for jet class events at 200 GeV.

3 Properties of selected jet events

In this chapter detailed characteristic of selected jet events ($CUT = 0.7$) are considered and compared with available information about jet properties from other processes.

Charged multiplicity of selected jet events as a function of $\sqrt{s}$ is shown in Fig. 18. It is compared with approximation of an average charged multiplicity measured in e^+e^- collisions [2], shown in Fig. 18 by a curve.

The mean kinetic energy of charged particles is shown in Fig. 19 along with approximation of mean momentum from e^+e^- collisions [2]. Though mean multiplicity in the selected spectator jet sample is of the same order as it is in e^+e^- collisions, mean energy of charged particles due to Lorentz factor is much higher than it is in e^+e^- collisions.

Contribution of different particles into jet average multiplicity and energy is shown in Table 1. Most of particles in spectator jets are charged pions and photons from π^0 -decays.

Important characteristic of selected jets is their shape which is determined by energy flow as a function of energy with respect to beam direction θ_{LAB}. Distributions of energy deposited in the ECAL and the HCAL as a function of θ_{LAB} are shown in Fig. 20 and Fig. 21, respectively. For energies above 200 GeV more then 99% of energy

Table 1: Total multiplicity (N_i) of different particles in a spectator jet and their fraction (E_i/E_{TOT}) in jet energy.

Particle	N_i	E_i/E_{TOT}
$\pi^{\pm}$	0.116E+02	0.774E+00
γ	0.188E+02	0.156E+00
$K^{\pm}$	0.430E+00	0.263E-01
$e^{\pm}$	0.312E+01	0.198E-01
n, $\overline{\text{n}}$	0.592E+01	0.155E-01
p, $\overline{\text{p}}$	0.130E+01	0.153E-01
K_L^o	0.217E+00	0.153E-01
K_S^o	0.155E+00	0.152E-01
Λ	0.765E-01	0.517E-02

deposition in the HCAL is within 23^o cone, and more then 90% of energy is within 6^o cone. For the ECAL at 200 GeV more then 96% of energy deposition in the ECAL is within 23^o cone, and more then 85% of energy is within 6^o cone. For both the ECAL and the HCAL more then 60% of energy is is within 2^o cone for beam energy 200 GeV or higher. So, spectator jets are indeed very collimated.

For collider experiments jet size is usually expressed by a cone size in η, ϕ space, where $\eta = -ln(tan(\theta/2))$ and θ, ϕ are polar and azimuth angles, respectively [4]. For central region η and θ are very close numerically since $\delta\eta/\delta\theta = -1/sin\theta$, and $sin\theta$ for central region of collider experiments is near unity. Typical cone size for jet selection is

$$R = \sqrt{\Delta\eta^2 + \Delta\phi^2} < 0.7 \quad . \tag{4}$$

The integrated fraction $E(< \theta_{LAB})/E_{TOT}$ of spectator jet energy measured by calorimeter in cone, limited by angle θ is shown in Fig. 22. Weights for the ECAL, the S2 and the HCAL compartments of the combined calorimeter were optimized for 200 GeV jets and are 1.113, 94.4 and 183.5, respectively. Due to calorimeter nonlinearity the measured energy does not approach exactly to the input energy E_{TOT}, when input energy is different from 200 GeV. The plateau in measured energy is reached for θ above 40^o or 0.7 radians if the input energy is above 200 GeV. These value (0.7 radians) agrees with typical jet cone size $R = 0.7$ [4]. For comparison integrated fraction $E(< \theta_{LAB})/E_{TOT}$ of pion energy in similar conditions is shown in Fig. 23. In case of pions the plateau is reached for θ above 20^o. This value of cone angle arise due to hadronic shower size and the distance from the target to the ECAL which is taken 317 cm according to the CMS TP [5].

Energy resolution of the combined calorimeter as a function of cone angle which limits its outer boundary is shown in Fig. 24 and Fig. 25 for jets and pions, respectively. Energy resolution $\delta E/E$ reaches its plateau for angles above 40^o and 10^o for jets and pions, respectively, and energies above 10 GeV. For energies above 200 GeV the plateau in resolution starts for $\theta > 20^o$ even for jets. This allows one to study at test beams calorimeter prototypes and modules of limited size as usually takes place. The distance between the target and the combined calorimeter could also be reduced for the purpose of test beam study.

Monte Carlo calculations of energy resolution for the CMS hadron calorimeter exposed with single particles and spectator jets have been made recently [3]. In particular, energy resolution of the Endcap hadron calorimeter at 200 GeV is 7.16% for single hadrons and 6.36% for spectator jets.

Experimental study of the CMS calorimeters at the proposed test beam experiment will allow to check the predictions, optimize final calorimeter structure, develop and tune jet finding algorithm.

4 Conclusion

It is shown that a simple trigger algorithm can be used to select spectator jets at test beam facilities. Selected events can be used to explore performance of different collider experiment detectors in a jet environment. These events can be used also for development and tuning of of jet selection algorithm and calorimeter calibration scheme. Properties of selected jets have been studied as a function of beam energy and angle of emitted particles. Predictions have been made for the CMS hadron calorimeter energy resolution for single particles and jets, which can be tested in fixed target experiment with the proposed jet trigger algorithm.

5 Acknowledgments

I am grateful to V.I.Kryshkin for helpful conversations and support.

References

[1] F.Garminati et al., **CERN Program Library (Dec.1991)**, *"GEANT User's Guide"*.

[2] B.H.Wiik, **preprint DESY 83-123, December 1983**. *"Detectors for quark and gluon jets at high energies"*

[3] V.V.Abramov, **CMS Note 1997/014**, *"CMS Endcap calorimeter energy resolution with additional active layers between ECAL and HCAL"*.

[4] H.Weerts, **FERMILAB-Conf-94/035-E**, *"Studies of Jet Production with the D0 Detector"*.

[5] CMS Collaboration. **CERN/LHCC 94-38, December 15, 1994.**, *"The Compact Muon Solenoid, Technical Proposal"*.

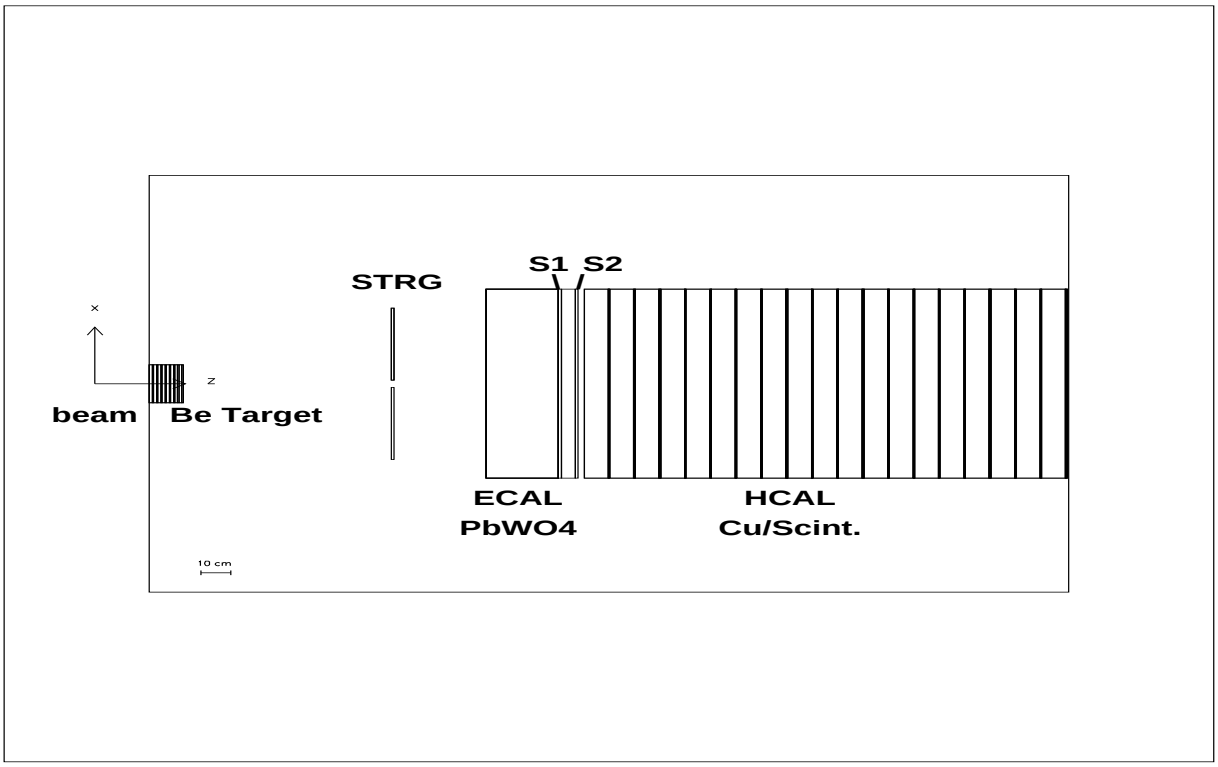

Figure 1: The schematic layout of a test beam facility. Hodoscope STRG and active target are used to make jet trigger. Jets or single particles are detected in a hadronic and an electromagnetic calorimeters.

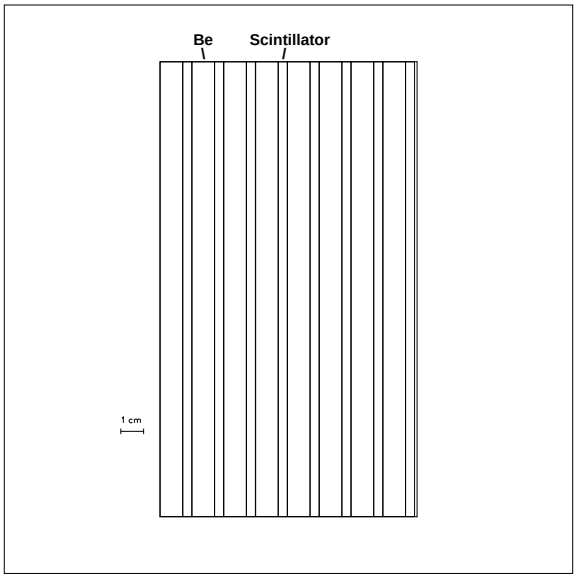

Figure 2: Schematic layout of the active target for jet events selection.

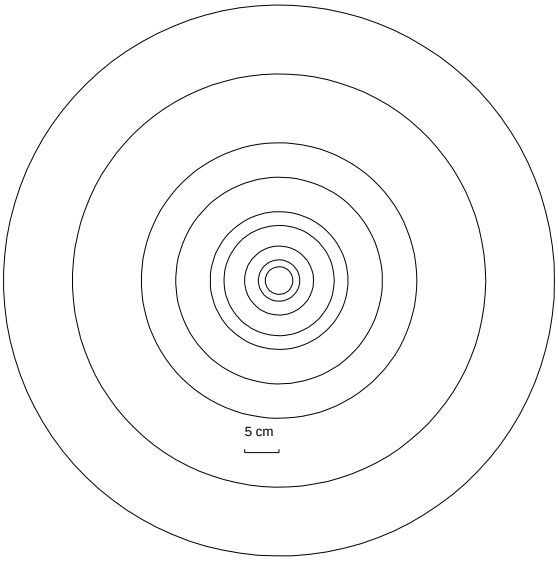

Figure 3: Schematic layout of the trigger hodoscope STRG.

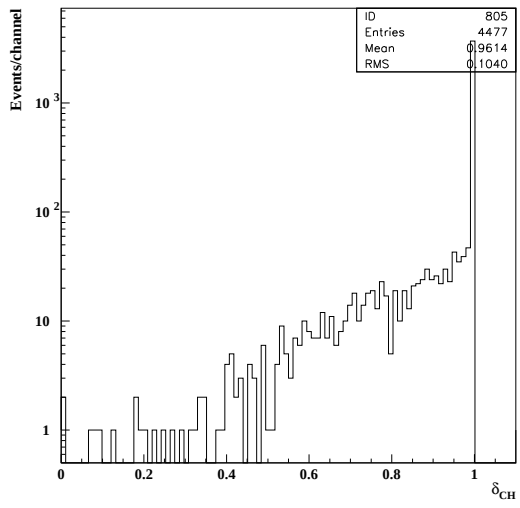

Figure 4: The ratio of kinetic energy of charged particles to the kinetic energy of all particles after the target at 200 GeV/c.

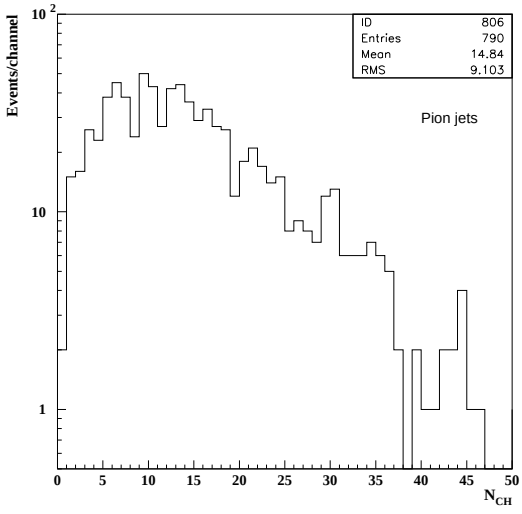

Figure 5: Charged multiplicity distribution for jet class events at 200 GeV/c.

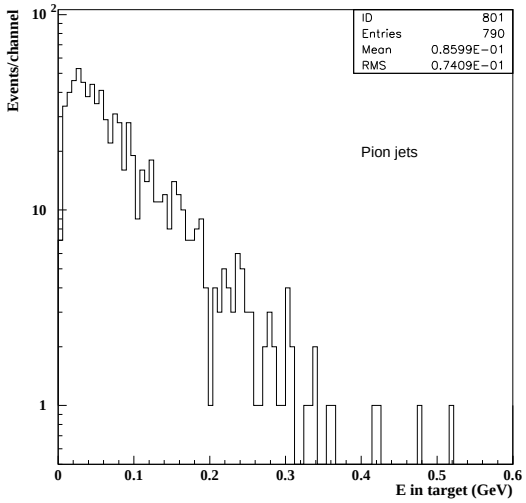

Figure 6: Energy deposition in the target for events with jet production by 200 GeV/c pions.

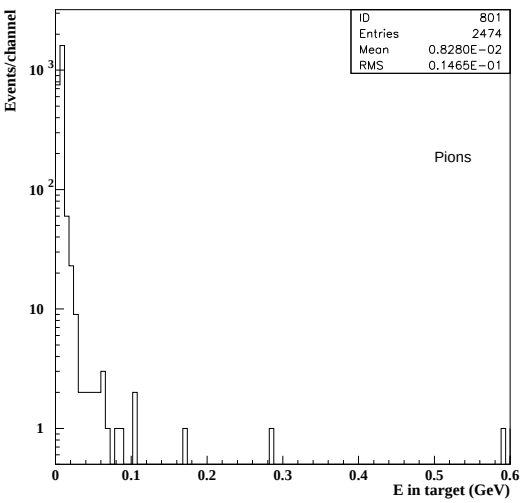

Figure 7: Energy deposition in the target for events without interaction of 200 GeV/c pions.

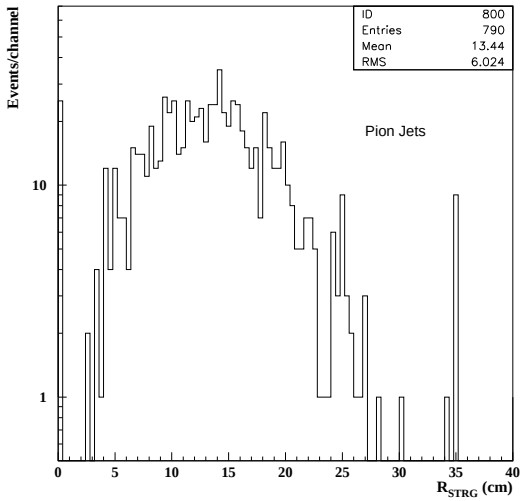

Figure 8: Average radius in hodoscope for events with jet production by 200 GeV/c pion beam.

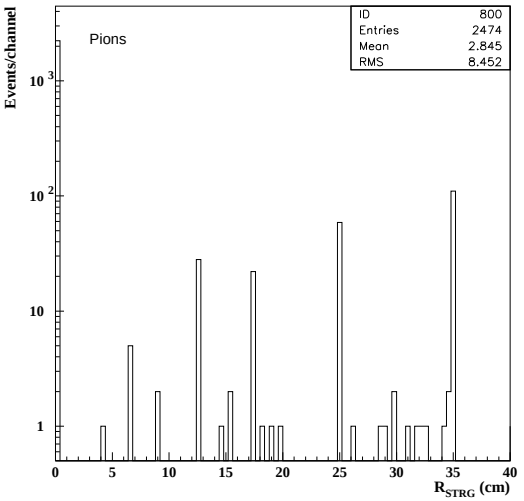

Figure 9: Average radius in hodoscope for single particle events and 200 GeV/c pion beam.

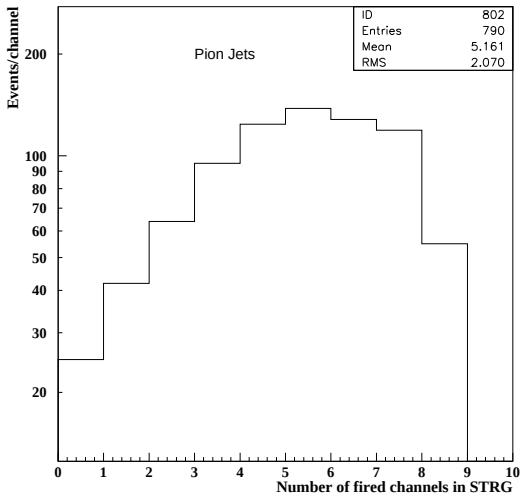

Figure 10: Number of fired channels in hodoscope for events with jet production by 200 GeV/c pion beam.

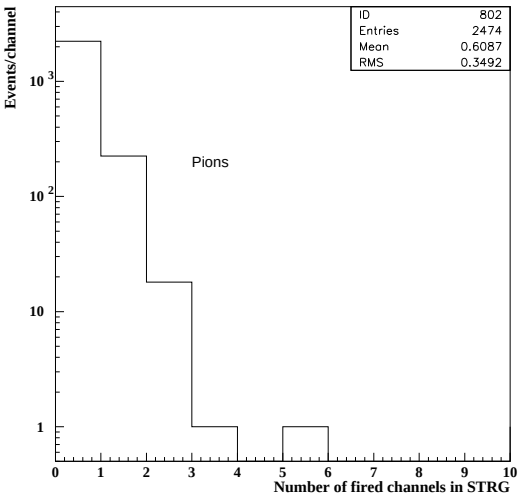

Figure 11: Number of fired channels in hodoscope for single particle events and 200 GeV/c pion beam.

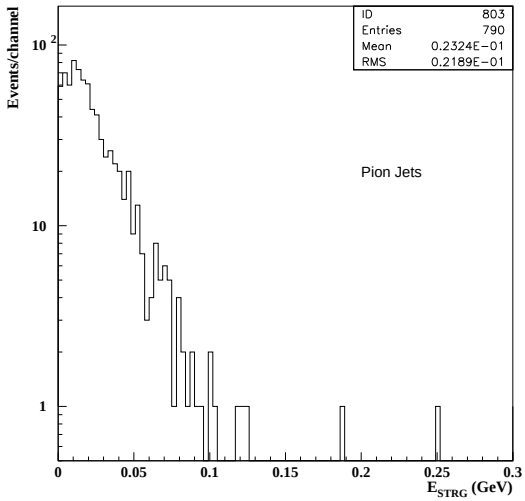

Figure 12: Energy deposition in hodoscope for events with jet production by 200 GeV/c pion beam.

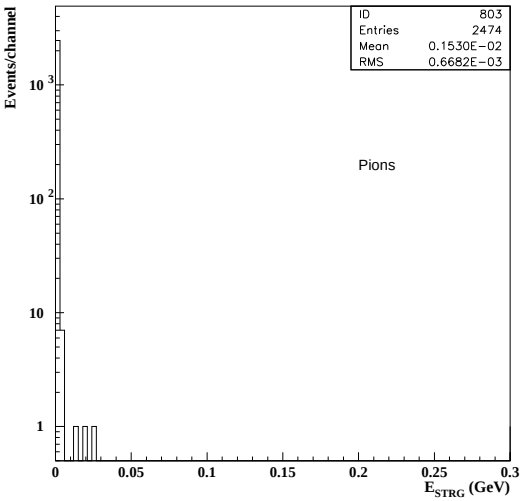

Figure 13: Energy deposition in hodoscope for single particle events and 200 GeV/c pion beam.

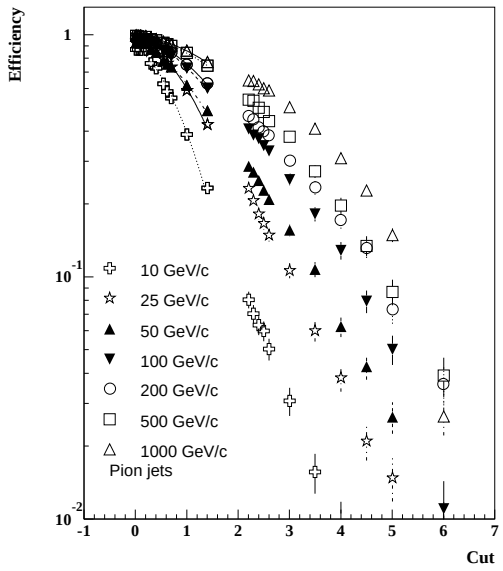

Figure 14: Efficiency for jet selection by combined algorithm for events with jet production by 200 GeV/c pion beam.

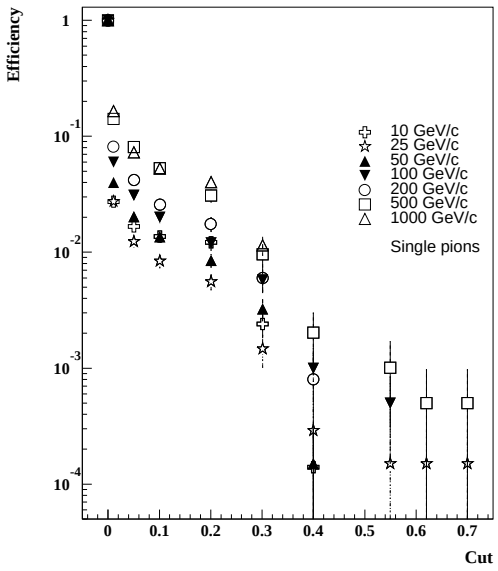

Figure 15: Efficiency of combined algorithm vs CUT for single particle events at 200 GeV/c pion beam.

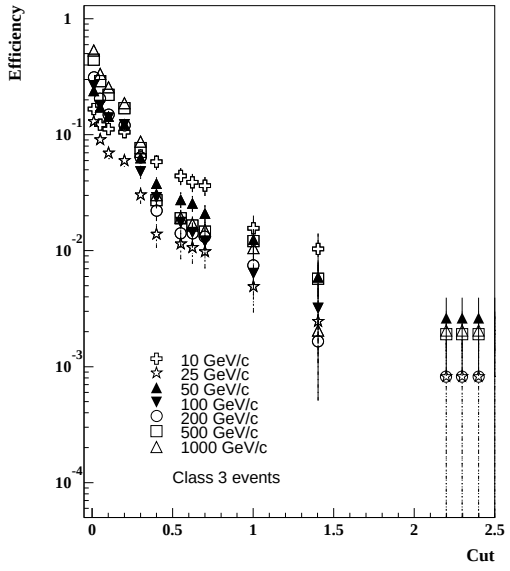

Figure 16: Efficiency of combined algorithm for class 3 events at 200 GeV/c pion beam.

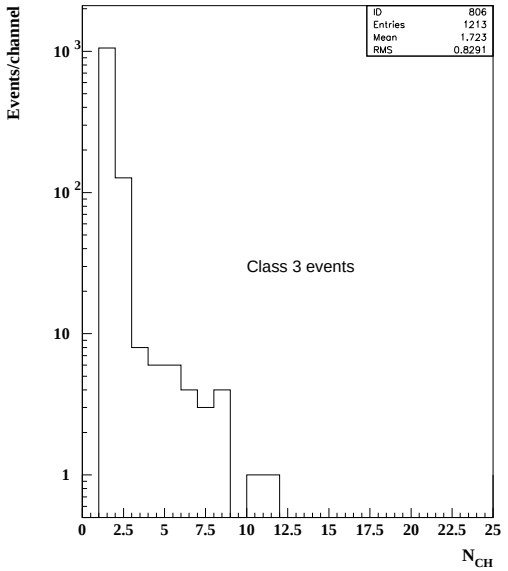

Figure 17: Charged multiplicity for class 3 events and 200 GeV/c pion beam.

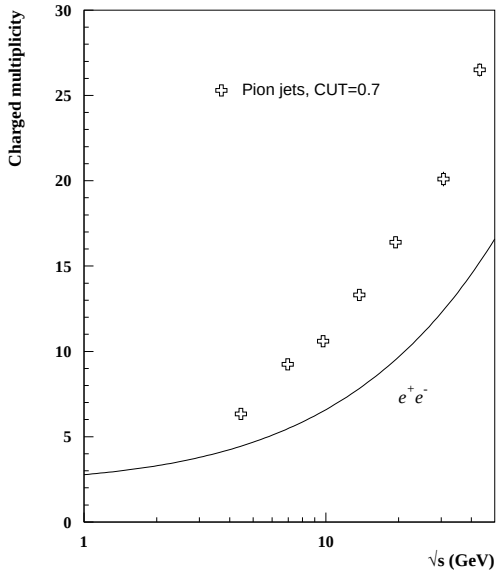

Figure 18: Charged multiplicity for events selected at $CUT = 0.7$. Curve shows charged multiplicity in e^+e^- collisions.

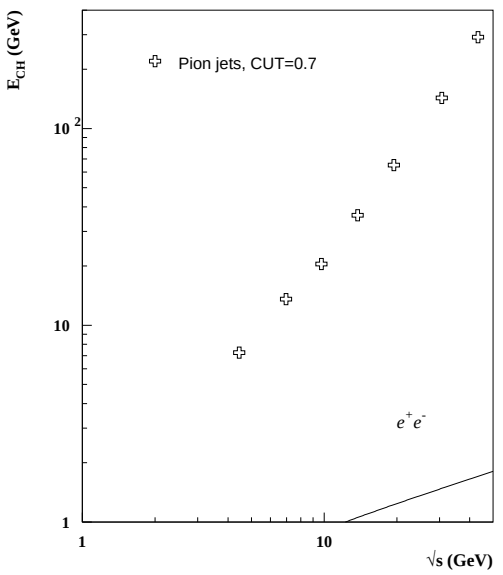

Figure 19: The mean kinetic energy of charged particles in events selected at $CUT = 0.7$. Curve shows approximation of mean momentum in e^+e^- collisions.

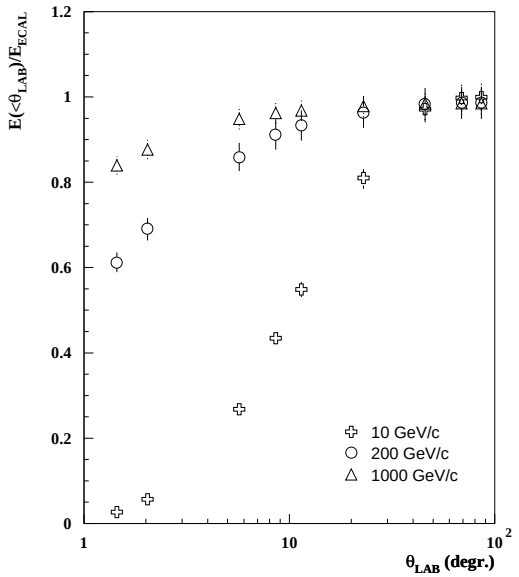

Figure 20: Distribution of deposited energy in the ECAL as a function of laboratory angle θ_{LAB}.

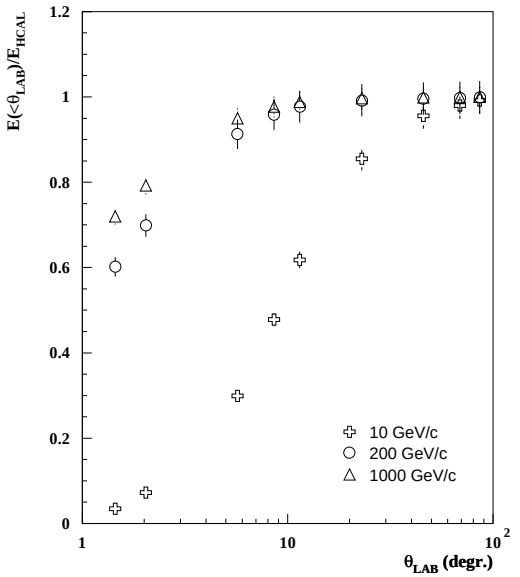

Figure 21: Distribution of deposited energy in the HCAL as a function of laboratory angle θ_{LAB}.

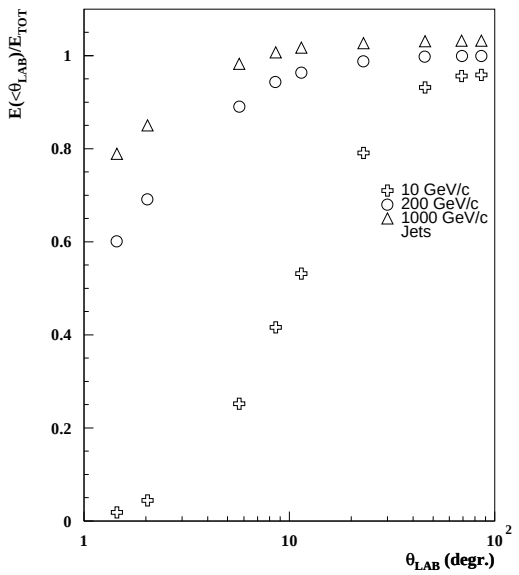

Figure 22: The ratio of measured energy to the input kinetic energy as a function of laboratory angle θ_{LAB} of cone limiting calorimeter size. Selected events are spectator jets produced by pions.

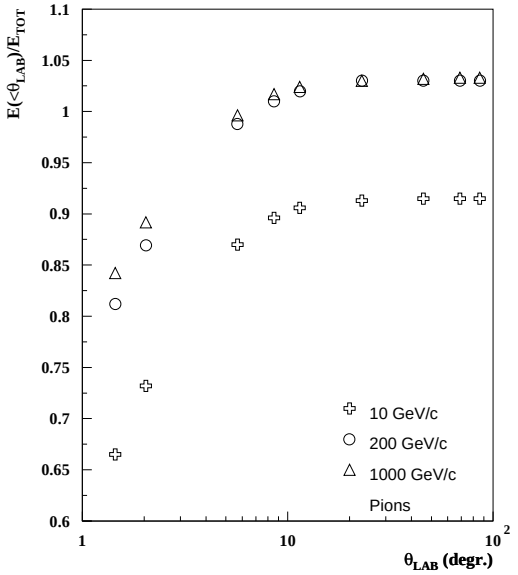

Figure 23: The ratio of measured energy to the input kinetic energy as a function of laboratory angle θ_{LAB} of cone limiting calorimeter size. Selected events are pions.

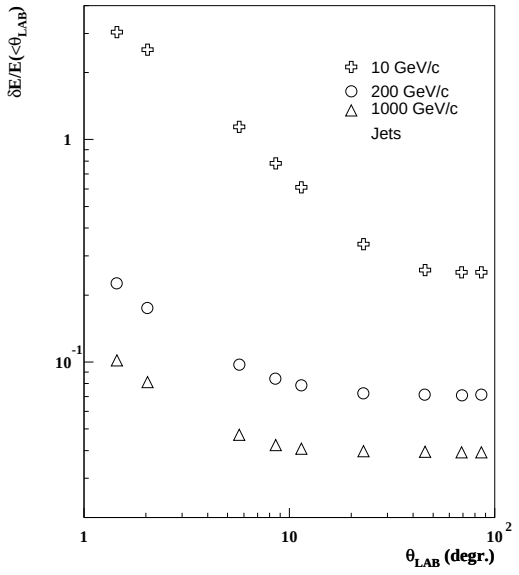

Figure 24: Relative energy resolution of combined calorimeter as a function of laboratory angle θ_{LAB} of cone limiting calorimeter size. Selected events are spectator jets produced by pions.

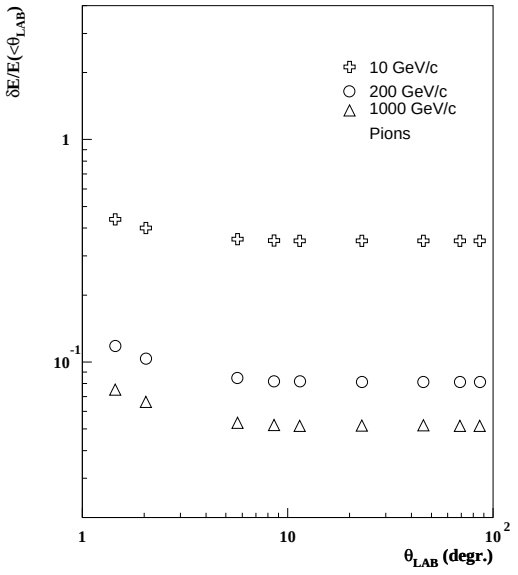

Figure 25: Relative energy resolution of combined calorimeter as a function of laboratory angle θ_{LAB} of cone limiting calorimeter size. Selected events are pions.